OVERVIEW OF EARLY RHESSI RESULTS

Säm Krucker and H. S. Hudson

Space Sciences Laboratory, University of California, Berkeley, USA

ABSTRACT

The RHESSI[1] spacecraft, launched in February 2002, provides imaging spectroscopy in the energy range 3 keV – 17 MeV. This energy range gives a general view of the many forms of solar activity observable with X-ray and γ-ray emission. In this paper we review some of the early results of RHESSI, including results on microflares and both hard X-ray and γ-ray observations of flares.

Key words: acceleration of particles – gamma rays: observations – Sun: flares – Sun: X-rays, gamma-rays.

1. INTRODUCTION

The solar corona exhibits many phenomena that involve particle acceleration and/or the production of plasmas at high temperatures. At the top end these include flares and coronal mass ejections (CMEs), but many kinds of small-scale activity also occur. Outside these impulsive processes a more or less steady corona exists, with temperatures ranging from about 10^6 K in coronal holes up to a few times 10^6 K in steady active-region loops. Parker's "nanoflare" concept identifies the heating of these hot but slowly-varying regions with energy release in many unresolved non-thermal processes associated with the formation of current sheets during the slow evolution of the structure.

RHESSI now gives us the most sensitive and highest-resolution observations yet of X-ray and γ-ray emissions from the solar atmosphere. As described more fully by Lin et al. (2002), the instrument consists of a nine-element array of hyperpure germanium detectors viewing the Sun through a set of modulation collimators. This results in a capability for imaging spectroscopy with angular resolution down to $2.26''$ (FWHM for the finest grids) and energy resolution ranging from about 1 keV (FWHM) for X-rays to a few keV for γ-rays. The instrument is also capable of high time resolution, limited by counting statistics, and has a novel system of movable absorbing shutters that give it large effective area at low energies during times of weak activity.

In this overview paper we discuss some of the results from the initial two years of RHESSI operations. The topics include microflares; the identification of sources of interplanetary electrons; the behavior of hard X-ray footpoint sources in flares; new observations of coronal X-ray sources; the first fully resolved observations of the γ-ray lines from inelastic scattering; the first imaging observations of the 2.2 MeV line from deuterium formation; and new opportunities for studying X-ray line emission features.

[1]The Reuven Ramaty High-Energy Spectroscopic Explorer

2. SUMMARY

2.1 Microflares

RHESSI observes large numbers of microflare events (Krucker et al., 2002; Liu et al., 2004). The term "microflare," as used here, refers to a tiny flare-like event, with the term "nanoflare" reserved for microscopic energy release in Parker's sense, if one wishes to make a physical distinction (Hudson, 1991). RHESSI observes microflares almost continuously, as illustrated in Figure 1. Can such events "heat the corona"? The answer to this question lies in the distinction between steady heating and flaring, and this in turn depends upon which part of the corona is discussed (e.g., Benz & Grigis 2002). At higher photon energies we mainly observe active regions because of spectral bias – this is the case in the X-ray band by GOES, *Yohkoh* SXT and other grazing-incidence soft X-ray telescopes, as well as RHESSI. Even in the active regions, though, time-series data such as that from GOES show clearly that either steady or flare-dominated variability dominates at different times. The large-scale corona and coronal holes generally show less time variability, have lower plasma temperatures, and are better observed with normal-incidence EUV instruments, such as EIT or TRACE.

The microflare examples in Figure 1, although only a few events out of a great many, illustrate an important point: the low-energy hard X-ray spectrum is ambiguous about the nature of its source. This is because bremsstrahlung, the mechanism of hard X-ray continuum emission, essentially integrates the spectrum of the radiating electrons in energy and therefore provides only a smoothed representation of it – a hypothetical sharp low-energy cutoff in the spectrum of non-thermal electrons will result in a gradual roll-off of the hard X-ray spectrum towards low energies. Even RHESSI's unprecedented energy resolution and excellent calibration cannot readily overcome this physical handicap. As the right panel of Figure 1 illustrates, the spectrum of the early "non-thermal" phase of the microflare might equally well be interpreted as a thermal component, albeit at a remarkably high temperature (29×10^6 K). Never-

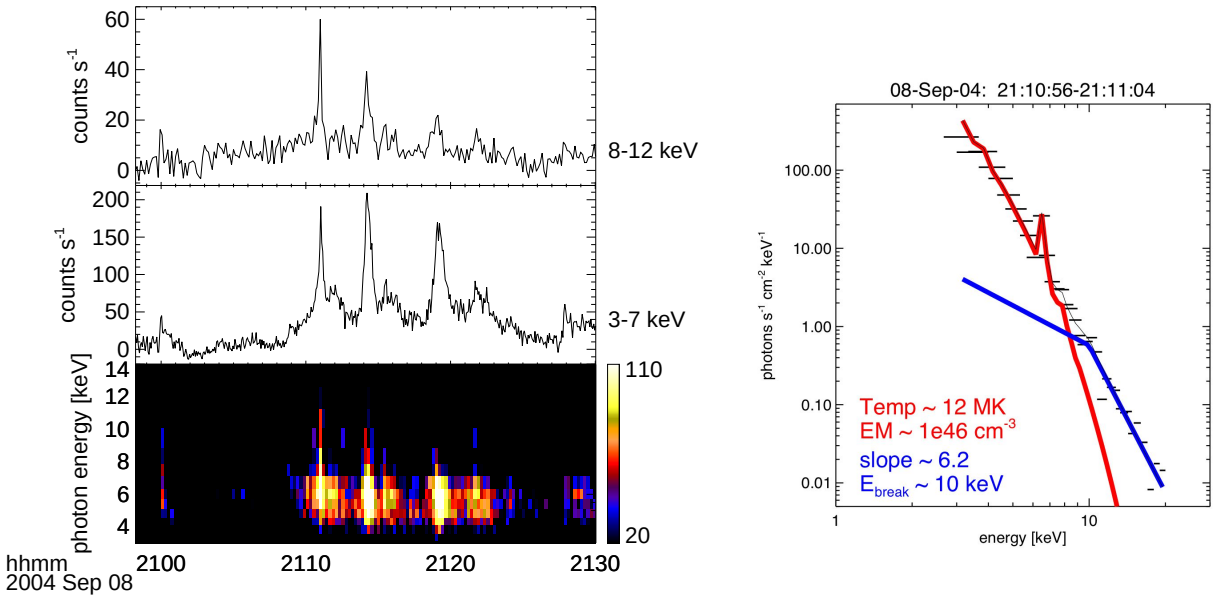

Figure 1. Solar microflare activity during SOHO Workshop 15, September 8, 2004: Left, RHESSI observations in the 3-20 keV range showing a series of at least six microflares. Top, time profile in the non-thermal range (8-12 keV); middle, time profile in the thermal range (3-7 keV); bottom, spectrogram representation of the same data. Right, spectrum of the hardest microflare during the shown time period occurring around 21:11 UT, corresponding approximately to GOES A0 with background correction. A thermal (red) and non-thermal (power law) fit (blue) is shown. Below the break energy, a slope of 1.7 is assumed. A fit with two thermal components gives a slightly worse fit, but is possible and gives an extremely high temperature of ∼29 MK for the hotter component with an emission measure of about 100 times smaller than the cooler component.

theless the RHESSI data show that microflares even at GOES A magnitudes involve either particle acceleration or "superhot" plasma temperatures.

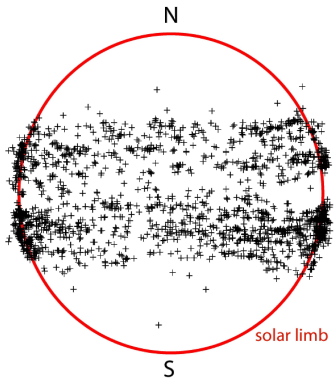

Figure 2. Distribution of RHESSI microflares on the solar disk, showing a strong tendency for association with active regions. This sample shows about 2,000 individual events obtained during a three-month span and may include a few erroneous positions.

The distribution of the total energies of the observed events reflects the potential of the events to account for the coronal luminosity, in the sense that a power-law distribution $W^{-\alpha}$ with $\alpha < 2$ will tend to concentrate the energy flow into the larger events, rather than the smaller ones. Such a flat distribution is well-known to hold for ordinary flares and microflares over a wide range of energies (e.g., Crosby et al. 1993). Characterizing the distribution at the low-energy end is difficult, and RHESSI results are not yet complete enough to cite here. The low-energy limit of the distribution function is particularly difficult to determine at "high" energies (> 3 keV for RHESSI). This would be needed to observe the tiny fluctuations that one might relate to nanoflares in the quiet corona or in quiescent active-region loops. The reason for this is instrument sensitivity – even RHESSI, with an effective area of $\sim$100 cm^2 at 6 keV, cannot detect the quiet Sun with short integration times.

2.2 HXR flares and escaping electrons

Because RHESSI provides the first clear view of the 3-10 keV band (clear because of large effective area and high resolution), we are finding evidence for the solar counterparts of energetic-particle events observed in the heliosphere. In principle this has always been possible: solar particles observed in interplanetary space have sufficient energies to create non-thermal bremsstrahlung (electrons) or inelastic-scattering γ-rays (ions) in the solar atmosphere where they originate. The problem is in the

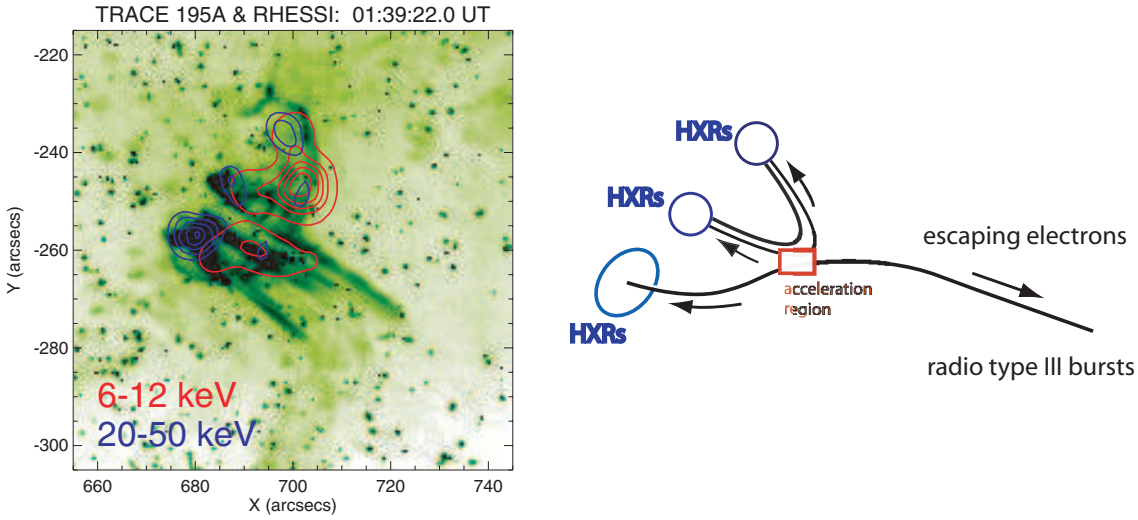

Figure 3. Solar source region of a flare (21 August 2002; M1.4, S11W47) releasing energetic electrons into interplanetary space that are later observed near Earth. The left panel shows RHESSI contours at 6-12 keV (red; thermal emission) and 20-50 keV (blue; non-thermal emission) overlaid on a TRACE 195Å EUV image (darker green corresponds to enhanced emission; the speckled appearance is due to particle background). Around (700, -245), the RHESSI contours clearly outline a soft X-ray loop with two hard X-ray footpoints. The strongest non-thermal source, however, is slightly to the southeast (683, -257) and is associated with a lower-intensity thermal source. The cartoon in the right panel interprets the event in the geometry described by Heyvaerts et al. (1977). The red box marks a plausible reconnection site from which downward-moving electrons could produce the HXR sources and upward-moving electrons could escape into interplanetary space. See Movie #1.

unknown density of this region, and in the sensitivity of the photon observations.

The example shown in Figure 3 illustrates this new development. A soft X-ray jet (Shibata et al., 1992; Strong et al., 1992) may occur in coincidence with the acceleration of electrons promptly observed near the Earth. These semi-relativistic electrons have short travel times and well-defined trajectories, so there is little ambiguity in the identification of the source. Jets appear to act as channels for meter-wave type III bursts (Aurass et al., 1994), so this identification with open field lines is reasonable. We thus find ourselves in a position to learn how the energy release involved in the flare/jet event relates to the magnetic structure that produces it. The right-hand panel of Figure 3 shows how this has developed, given the hard X-ray (footpoint) and soft X-ray (loop) observations in the left panel. The TRACE image in the background shows the connectivity with higher resolution. The hard X-ray footpoint source to the S appears appears isolated from the bright double-footpoint loop developing to the N, while the jet appears to emerge from both together.

Our cartoon representation of this resembles the geometry suggested for emerging flux by Heyvaerts et al. (1977), in which closed magnetic fields reconnect with open fields. We identify the particle escape with this reconnection process, either as a direct result of particle acceleration in the reconnection region, or as a mechanism by which particles can cross from open to closed fields. The latter interpretation seems more probable given the larger number of electrons typically required for the flare hard X-ray emission; otherwise one might expect comparable numbers of trapped and escaping electrons. The details of the SEP generation remain incompletely known: the TRACE view of the jet in Figure 3 shows a complicated geometry not well represented in the cartoon. The location and conditions of the reconnection process remain to be studied, but it is clear that the open magnetic field lines that allow particle escape must already have been present close to the site of the flare prior to the event.

2.3 HXR footpoints

RHESSI imaging spectroscopy in the hard X-ray range shows the independent development of footpoint and loop sources, as in the X-class flare of 23 July 2002 flare (Emslie et al., 2003). The behavior of the hard X-ray footpoints in such flares allows us a more detailed view of the coronal development based on a standard model of large-scale reconnection. Figure 4 shows sequences of footpoints in the 23 July 2002 event (Krucker et al., 2003). The centroid positions determined from the RHESSI images are much more precise ($\sim$0.2″ RMS for 8 s integrations) than the angular resolution of the imager, and show well-resolved apparent motions. The motions presumably are not physical, but instead represent a conflagra-

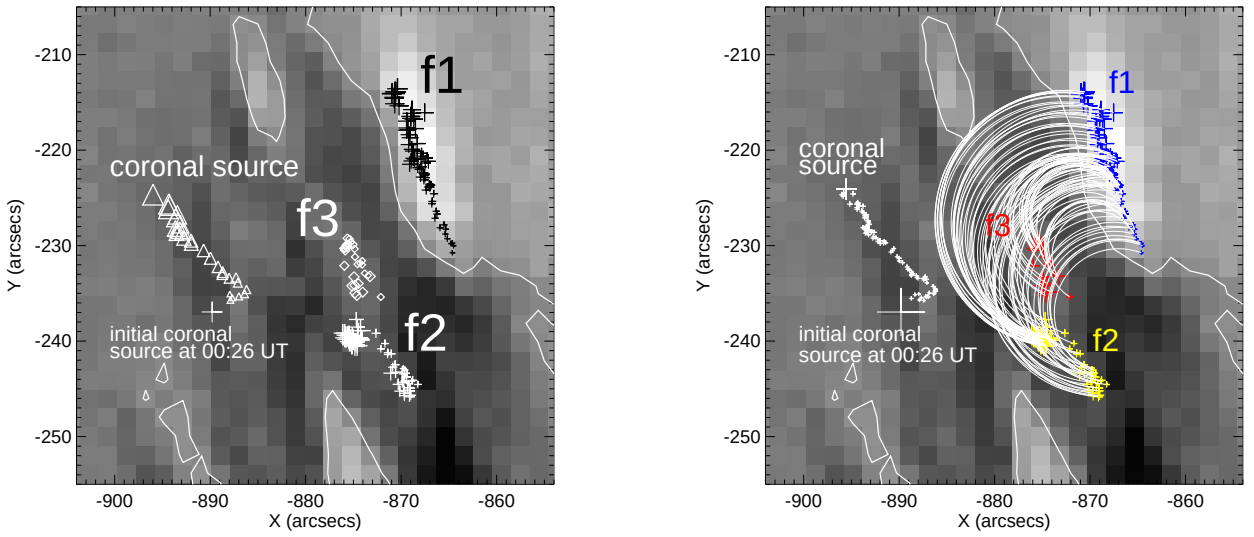

Figure 4. Left: temporal evolution of the HXR footpoints f1 (black crosses), f2 (white crosses), and f3 (white diamonds) at 30–80 keV and the coronal source (white triangles) at 18–25 keV. The centroid positions of the different sources taken every 8 seconds for the footpoints and every 26 seconds for the coronal source are shown on an MDI magnetogram in which the apparent neutral line is shown in white; extreme line-of-sight values are ±600 G. The increasing size of the symbols represents times from 00:26:35 to 00:39:07 UT. The centroid of the early-phase coronal source at 00:26 UT is marked with a white cross (from Krucker, Hurford, & Lin 2003). Right: same as to the left, with semicircles connecting simultaneously brightening footpoints. The semicircles form an arcade of loops. The coronal source seems to be at higher altitude than the tops of these loops. See Movie #2.

tion wave of successively excited coronal field lines, at their roots in the chromosphere. The "looptop" sources are different and (in this flare) appear to reveal physically distinct features early and late in the flare. In the early phase (labeled "initial coronal source") little chromospheric evaporation can have occurred, and it is not clear how the dense medium required for detectable bremsstrahlung radiation has developed. In the later phase, as illustrated by the sketches (ad-hoc semicircles) of interconnecting loops, the coronal source seems to lie outside these idealized features and at a higher altitude.

The footpoint motions follow the pattern expected for coronal magnetic reconnection and allow a crude estimate of the reconnection rate (Sakao et al., 1998; Fletcher & Hudson, 2002; Qiu et al., 2002; Krucker et al., 2003). Figure 5 confirms that the flare brightening and the footpoint motions indeed do correlate, consistent with a close relationship between energy release and particle acceleration and large-scale coronal magnetic reconnection.

2.4 Coronal hard X-ray sources

The subject of coronal hard X-ray sources is an important one for RHESSI because of the wealth of other information (radio and particle observations, in particular) that assure us of the presence of nonthermal electrons in the low corona. Such observations are difficult because of the large dynamic

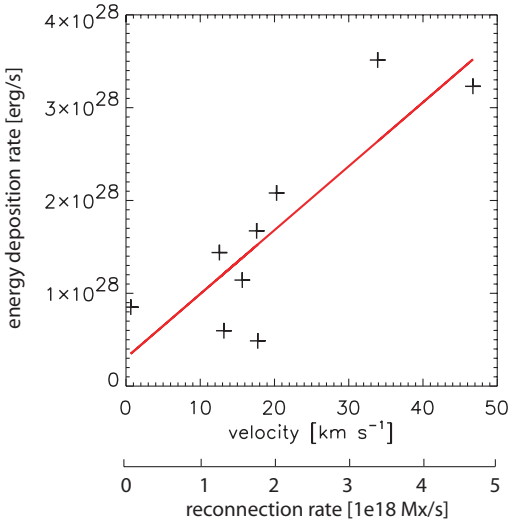

Figure 5. Temporal correlation of the footpoint motion and the energy deposition rate in the northern footpoint during the July 23, 2002 event. For this near-the-limb flare, the magnetic field strength in the footpoint is not well observed, but simply assuming a constant field strength of 1000 G enables us to interpret the observed velocity as a reconnection rate as given at the bottom of the figure.

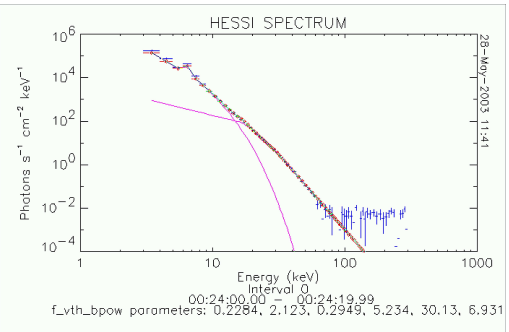

Figure 6. Spectrum of the early coronal source that developed prior to the impulsive phase of the 23 July 2003 event. This spectrum does not show a strong high-energy tail, but does include the standard features of the typical thermal-plus-nonthermal fits: an iron feature at about 6 keV and a "knee" in the spectrum at about 30 keV. Because this observation precedes the impulsive phase, little evaporation can have happened (see Holman et al., 2003, and Lin et al., 2003, for further details).

range needed to separate the brighter chromospheric sources from the fainter coronal ones. For examples of observations prior to RHESSI see Cliver et al. (1986), Masuda et al. (1994), and Hudson et al. (2001).

The γ-ray event of 23 July 2002 gave us a chance to an interesting hard X-ray sources in the corona above the site of the flare, but prior to its impulsive phase. In Figure 4 one can see that the location of the source did not match that of the loop-top sources developing in the main phase of the flare. Footpoint sources were not prominent during this development, suggesting that the non-thermal electrons remained in the corona and were somehow able to dissipate their energy without strong chromospheric counterparts. Lin et al. (2003) give further details regarding this observation. See Movie #3 for a dynamic view of this early phase of the flare development.

2.5 Evidence for a current sheet?

Another RHESSI contribution to our understanding of the, coronal development of a flare comes from observations argued to represent a coronal current sheet (Sui & Holman 2003). Observations of this kind follow in the direction pioneered by the *Yohkoh* discovery of a coronal hard X-ray source during the impulsive phase of the Masuda flare (Masuda et al. 1994). Figure 7 shows RHESSI and TRACE images of a flare of 15 April 2002, one of a series of events with similar behavior. The key finding is not the hard X-ray source as such, although the left panel of Figure 7 shows (blue contours) a feature consistent with the Masuda flare; instead the RHESSI images in the right panel show an *inverse* temperature dependence in the thermal X-ray domain. The typical pattern of loop-top sources reveals a temperature increasing with height, which itself is consistent with the standard model of sequential magnetic reconnection onto longer and longer field lines as the reconnection point rises in the corona.

The inverse temperature gradient observed in the 15 July 2002 event suggests that it and the simultaneous loop-top source, with a normal temperature gradient, form the ends of a large-scale current sheet above the flare loops. Thus Sui & Holman (2003) argue that this provides further evidence for a standard reconnection theory (e.g., Priest & Forbes 2002). Veronig & Brown (2004) point out that the density inferred from the soft X-ray loop structure in this case corresponds to a *collisionally thick* medium up to an energy of some 60 keV.

These events and the 23 July 2003 rise-phase event discussed in the previous section considerably extend the observations of coronal hard X-ray sources, but the RHESSI data have not yet provided good examples of earlier types (the Masuda flare, for example). This probably means that a rich variety of coronal hard X-ray sources does exist, as we would expect from other kinds of observation, and so we look forward to fuller analysis of the RHESSI database in this area.

2.6 Nuclear emission lines

The solar γ-ray spectrum consists of several line and continuum components, generally visible only during flares (Chupp, 1984; see Lin et al., 2002, for an overview of RHESSI's capabilities). The lines are (i) the inelastic scattering lines, produced by direct excitation of nuclear excited states via ion-ion collisions, (ii) the 0.511 MeV line from positron annihilation, for which the positrons are secondaries from other ion-ion collisions; and the 2.223 MeV line of deuterium formation, from thermalizing secondary neutrons. RHESSI has observed all of these components, with unprecedented spectral resolution, in several events (see papers in ApJL, 595, 2003). This resolution is adequate to resolve all of the de-excitation lines, including especially the narrow-line component from the target ions plus the 0.511 MeV positron line, but not the very bright neutron-capture line at 2.223 MeV. RHESSI also provides limited imaging of these γ-ray lines. The de-excitation lines show persistent redshifts in rough accordance with the nuclear masses for the narrow-line component (Smith et al., 2003), as shown in Figure 8.

The 0.511 MeV line of positron annihilation has provided one of the bigger surprises from RHESSI's γ-ray observations to date. Its line width appears to require a thermal origin at transition-region temperatures (Share et al., 2003). Obviously it would be difficult to maintain – for many minutes – a thick layer at such a temperature. The region must be thick enough, with column depths exceeding 10^{24} cm^{-2}, to be able to stop not only the primary ions, but

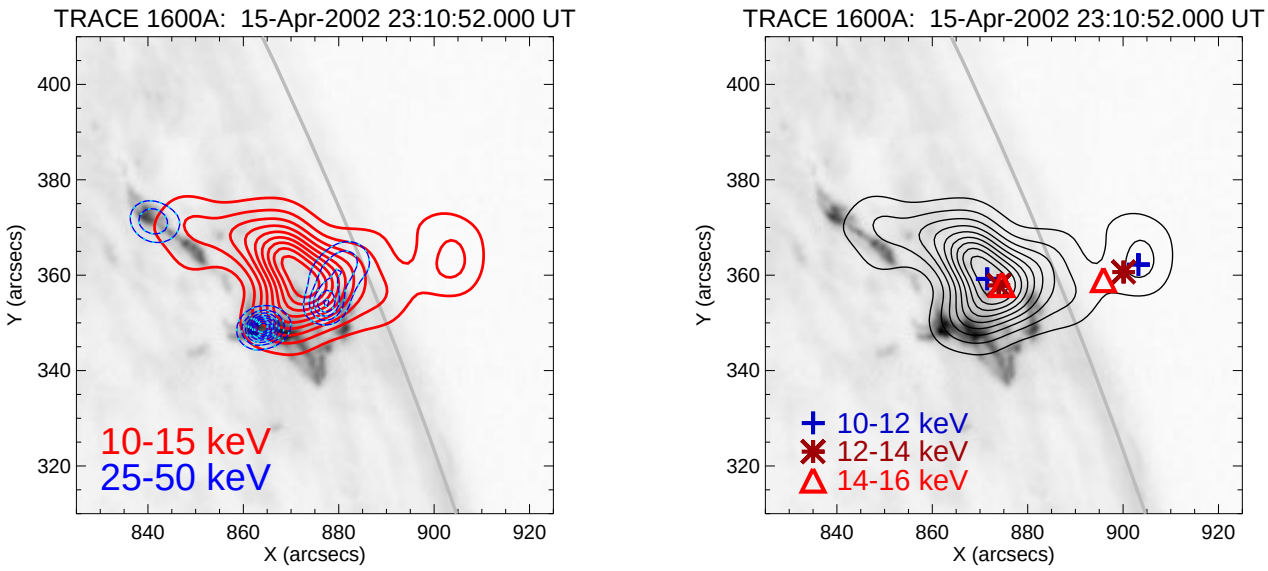

Figure 7. (left) RHESSI X-ray observations of the flare occurring on April 15, 2002 around 23UT showing a cusp-like structure in the 10-15 keV thermal emission (red contours) with a separated source around (905/360). HXR emission (dashed blue) is seen from two footpoints (840/370) and (865/350) plus a third source around (880/355) that is possibly located in the corona. The underlying image is from TRACE taken with the 1600 Å filter. (right) The same figure without the HXR contours showing additionally the source position of the thermal emission at different energies as given in the lower (after Sui & Holman 2003; see text for details).

also the MeV-range secondary positrons. A satisfactory explanation of this interesting observation is not available at present.

2.7 Imaging of the 2.2 MeV line emission

The RHESSI γ-ray imaging uses only coarse collimators, and thus does not provide the high resolution and image dynamic range available for the hard X-rays. In addition, the count rates are low. Accordingly the only γ-ray imaging done to date consists of centroid determination for the 2.2 MeV line (Hurford et al., 2003, 2005). Because it depends upon secondary particle production during the interactions that produce γ-rays, it originates close to the sources of the inelastic-scattering and 0.511 MeV lines. We show an example of this imaging in Figure 9 (Hurford et al., 2005). This flare, that of 28 October 2003, reveals two γ-ray footpoints embedded in the flare ribbons (as seen by TRACE and in RHESSI hard X-rays). Although close to the hard X-ray centroid positions, each γ-ray footpoint is displaced to the east; the footpoint locations do not appear to imply a different loop length for ion acceleration as suggested by Emslie et al. (2004) for the event of 23 July 2004. This image comparison is differential, in the sense that RHESSI permits a choice of image-synthesis parameters that match at the two energy ranges, i.e. the use of an artificially low-resolution hard X-ray image made with only the γ-ray grids. Figure 9 actually shows contours from a higher-resolution hard X-ray image.

2.8 Iron X-ray emission feature

The K-shell transitions of Fe are strongly excited in a hot plasma, especially as lithium-like and higher ionization states appear. Phillips (2004) has used the CHIANTI atomic-physics database to describe the expected RHESSI spectrum in the 4-10 keV range (Figure 10) as a function of temperature. This shows a sharp turn-on of Fe feature emission at about 8 MK, and the growth of an Fe-Ni feature at slightly higher energies. Both of these features appear in the RHESSI spectra, as predicted by these model calculations. Because of its large effective area, RHESSI obtains excellent signal-to-noise ratio in this region; the Fe feature is not resolved but the centroid, peak emission energy, equivalent width, and strength can be determined with high precision and as a function of time. Figure 11 shows observations of a weak impulsive flare (GOES C1.1) to illustrate this capability.

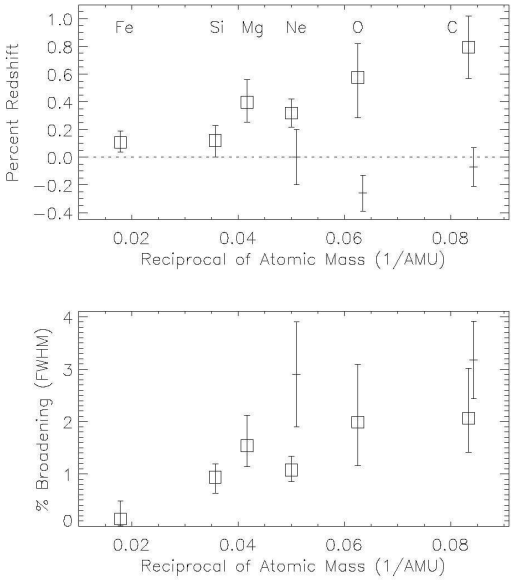

Figure 8. Redshift (top) and Doppler broadening (bottom) plotted as a function of the reciprocal of the nuclear mass. Data points marked as squares are from the 23 July 2002 flare. Data points marked with dashes are the average of five flares observed by SMM/GRS near 74° heliocentric angle (from Smith et al., 2003).

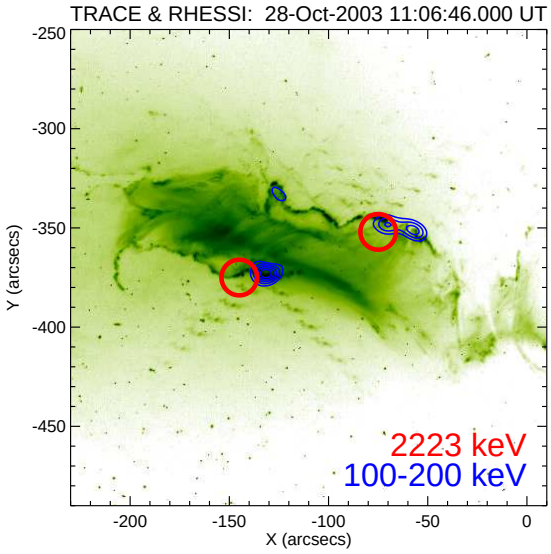

Figure 9. Imaging of the 2.2 MeV neutron capture line and HXR electron bremsstrahlung of the October 28, 2003 flare (Hurford et al., 2005). Superposed on a TRACE EUV 195Å image the event-averaged 2.2 MeV centroid positions (red circles) and the 100-200 keV electron bremsstrahlung contours around 11:06:46UT are shown. Both emissions are related to flare ribbons seen in EUV with TRACE.

3. CONCLUSIONS

RHESSI has performed nearly flawlessly during its first 2.5 years in orbit, during which many X-class flares have occurred. Among the surprises in its data has been the persistent detection of low-energy hard X-radiation in the 3-10 keV band, which at quiet times is dominated by microflaring. At the very quietest times even this signal disappears, but it is clear that even minimal levels of coronal activity immediately bring non-thermal and high-temperature plasma processes into play. At the time of writing we expect a further decline of activity for perhaps two more years, and it will be interesting to follow this newly-found hard component of X-ray emission during this time. Equally interesting will be deep searches for quiet-Sun events perhaps associated with the heating of the general corona or with the magnetic reconnection required for the development of coronal holes at low latitudes.

From launch the entire RHESSI database and the full software suite have been in the public domain, RHESSI has a near-monopoly on solar high-energy observations for the foreseeable future. Such observations are centrally important to most forms of solar magnetic activity, and we encourage additional users of the data. The RHESSI investigators conduct extensive workshop series, including hands-on workshops for training in data analysis. Please see the links on http://hessi.ssl.berkeley.edu/ for further information.

ACKNOWLEDGEMENTS

RHESSI is named for the late Reuven Ramaty, a co-investigator and a pioneer in the fields of solar physics, γ-ray astronomy, nuclear astrophysics, and cosmic rays. This research is supported in part by NASA contract NAS5-98033.

REFERENCES

Aurass H., Klein K.-L., Martens P. C. H., 1994, Solar Phys. 155, 203

Benz A. O., Grigis P. C., 2002, Sol. Phys. 210, 431

Crosby N. B., Aschwanden M. J., Dennis B. R., 1993, Sol. Phys. 143, 275

Chupp E. L., 1984, ARA&A 22, 359

Cliver E. W., Dennis B. R., Kiplinger A. L., Kane S. R., Neidig D. F., Sheeley N. R., Jr., Koomen, M. J., 1986, ApJ, 305, 920

Emslie A. G., Kontar E. P., Krucker S, Lin R. P., 2003, ApJ 595, L107

Emslie A. G., Miller J. A., Brown J. C., 2004, ApJ 602, L69

Fletcher L., Hudson H. S., 2002, Solar Physics, 210, 30

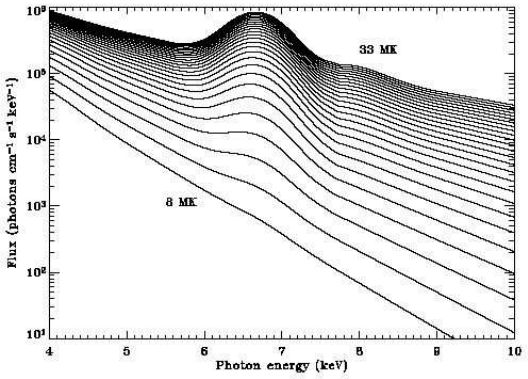

Figure 10. Model calculations of the X-ray emission spectrum in the 4-10 keV range from the CHIANTI compilation (Phillips, 2004). The 6-keV feature due to Fe K-shell transitions turns on at about 8 MK for a thermally relaxed plasma, and an 8 keV feature begins to appear at still higher temperatures. The model calculations assume coronal abundances and a spectral resolution of 0.8 keV.

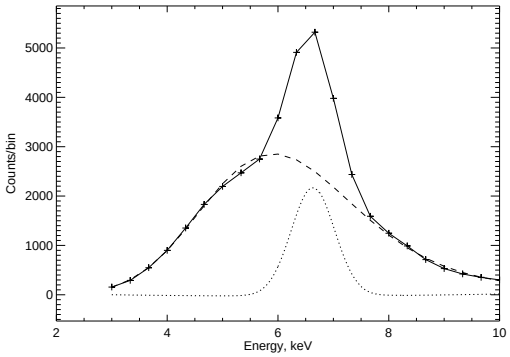

Figure 11. Decomposition of the RHESSI 3-10 keV spectrum for a 20-sec integration (1 February 2003, 00:39:40–00:40:00 UT) at the peak of a C1.1 impulsive flare. The solid line is the total fitted spectrum; the dotted line shows the (solar) background derived from a fourth-order polynomial fit to the logarithm of the RHESSI counts on 1/3 keV energy bins, excluding the energy range 5.67-7.33 keV of the Fe feature; the dashed line shows a Gaussian fit to the residuals.

Heyvaerts J., Priest E. R., Rust D. M, 1977, ApJ 216, 123

Holman G. D., Sui L., Schwartz R. A., Emslie A. G., 2003, ApJ 595, L97

Hudson H. S., 1991, Solar Phys. 133, 357

Hudson H. S., Kosugi T., Nitta N. V., Shimojo M., 2001, ApJ 561, 211L

Hurford G. J., Schwartz R. A., Krucker S., Lin R. P., Smith D. M., Vilmer, N., 2003, ApJ 595, L77

Hurford G. J., et al., 2005, in preparation

Krucker S., Christe S., Lin R. P., Hurford G. J., Schwartz R. A., 2002, Sol. Phys. 210, 445

Krucker S., Hurford G. J., Lin R. P., 2003, ApJL, 595, L103

Lin R. P., et al., 2002, Solar Physics 210, 3

Lin R. P. et al., 2003, ApJ 595, 89L

Liu C., Qiu J., Gary D. E., Krucker S., Wang, H, 2004, ApJ 604, 442

Masuda S., Kosugi T., Hara H., Tsuneta S., Ogawara Y., 1994, Nature 371, 495

Phillips K. J. R., 2004, ApJ 605, 921

Priest E. R., Forbes T. G, 2002, Astronomy Astrophysics Revs. 10, 313

Qiu J., Lee J., Gary D. E., Wang H., 2002, Apj 565, 1335

Sakao T., Kosugi T., Masuda S., 1998, ASSL 229, 273

Share G. H., et al. 2003, ApJ 595, L855

Shibata K., et al., 1992, PASJ 44, 173L

Smith D. M., Share G. H., Murphy R. J., Schwartz R. A., Shih A. Y, Lin R. P., 2003, ApJ 595, L81

Strong K., Harvey K., Hirayama T., Nitta N., Shimizu T., Tsuneta, S., 1992, PASJ 44, 155L

Sui L., Holman G. D., 2003, ApJ 596, 251L

Veronig A. M., Brown J. C, 2004, ApJ 603, L117